Chapter 13
Iron Oxide-Based Heterogeneous Catalysts for Environmental Applications

M. Roshni, S. Anaina, and D. Jagadeesan

Abstract Heterogenous catalysts based on iron are widely used in environmental remediation reactions due to their abundance and less toxicity. The prospects of upscaling and the risks of leaching during the treatment processes are important considerations to choose iron-based materials. Particularly, various forms of iron oxides, doped forms, iron oxyhydroxides in bulk and nanoforms are increasingly used for catalysis of environmental remediation. In this chapter, we have given the overview of these minerals and general variety of their usage in environmental catalysis. The applications of these iron-based materials in environmentally important reactions such as oxidation of volatile organic compounds (VOCs) and CO, selective catalytic reduction of NO_x and Fenton reaction are described.

Keywords Iron oxides · Thermal catalysis · Photocatalysis · Photothermal catalysis · Plasma catalysis · VOC oxidation · CO oxidation · Selective catalytic reduction of NOx · Fenton process

13.1 Introduction

Iron is the fourth most abundant element on earth constituting nearly 5 wt% of the earth's crust. The most dominant forms of iron are oxyhydroxide, oxides and sulfides. It is not only an important component of the functional proteins in living systems but has been an integral part of the civilizations since the iron age [1]. Iron oxide-based materials have been used in catalysis, biomedicine, environmental

M. Roshni · S. Anaina · D. Jagadeesan (✉)
Department of Chemistry, Indian Institute of Technology Palakkad, Ahalia Integrated Campus, Kozhipara, Palakkad, Kerala 678 557, India
e-mail: d.jagadeesan@iitpkd.ac.in

D. Jagadeesan
Environmental Sciences and Sustainable Engineering Centre (ESSENCE), Indian Institute of Technology Palakkad, Ahalia Integrated Campus, Kozhipara, Palakkad, Kerala 678 557, India

H. Sahoo and J. K. Sahoo (eds.), *Iron Oxide-Based Nanocomposites and Nanoenzymes*, Nanostructure Science and Technology, https://doi.org/10.1007/978-3-031-44599-6_13

remediation and energy storage devices due to their unique chemical, thermal, optical, electronic and magnetic properties. Among the 16 available oxide forms, haematite (α-Fe_2O_3), maghemite (γ-Fe_2O_3) and magnetite (Fe_3O_4) are the most studied ones. Haematite is the most stable form, which acts as a precursor for other oxides. It is an *n*-type semiconductor with a bandgap of 2.1–2.3 eV, whereas magnetite has very low resistivity and lower bandgap of 0.1 eV. Owing to its high abundance, low toxicity, high sensitivity/activity and high corrosion resistance, haematite is most widely used. In α-Fe_2O_3, Fe^{3+} occupies two thirds of octahedral sites with oxygen in hexagonal close packed arrangements, while in Fe_3O_4, oxide ions are in cubic close packed array resulting in an inverse spinel structure with Fe^{2+} in half of octahedral sites and Fe^{3+} in remaining octahedral and tetrahedral sites. The second most stable oxide of iron is γ-Fe_2O_3, which has a cubic spinel structure, where oxygen ions are in cubic close packed array and Fe^{3+} occupies the octahedral and tetrahedral sites [2] (Fig. 13.1).

An ever-increasing population coupled with aspirations for higher living standards has a direct or indirect impact on the air quality. Natural events and anthropogenic activities also release air pollutants in significant amounts making respiratory diseases as one of the major causes for death in recent years. The management of air quality is a perennial challenge that not only requires strict enforcement of policy level decisions but also development and deployment of new and efficient technologies to continuously monitor and curb it at the source. As clean air is an absolute necessity for a healthy living, the necessity to mitigate contaminants from the air has assumed enormous significance in recent decades. VOCs, CO, NO_x and particulate matter arising from the combustion of fossil fuels by stationary and mobile sources are major pollutants that must be mitigated. CO is not only a toxic gas upon inhalation but also aids in the formation of ground level ozone, which leads to severe environmental pollution. Similarly, brownish nitrogen oxides are also poisonous and affect respiratory system. Along with VOCs, NO_x creates photochemical smog during hot summer. The reaction between VOC and NO_x occurs in the presence of sunlight producing brownish haze. In the recent years, air pollution has significantly increased even indoors. In developing countries, indoor air pollution has outgrown outdoor pollution such that it causes 2 million deaths every year [3]. Indoor air contains particulate matter and VOCs, which originates from construction materials, cooking, furniture and different packing materials, which are considered as serious air pollutants. Different government agencies have their own measures and policies to

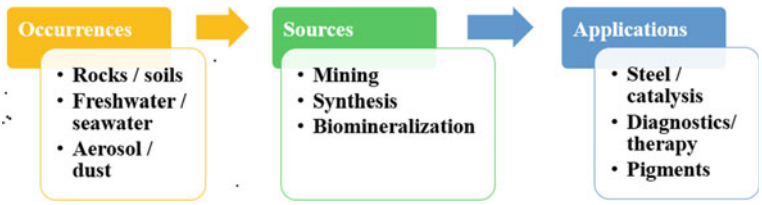

Fig. 13.1 Occurrence, sources and general applications of iron oxide [1]

reduce and mitigate gaseous emissions. For mitigating the emissions, thermal incineration systems or catalytic systems can be used. Catalytic systems are more preferred over incineration because of low energy demand. Lots of research worldwide are trying to develop an efficient thermal/photo/plasma/electrocatalytic system, which can mitigate air pollutants at the ambient conditions. Iron-based catalytic materials have successfully found their way to play a reliable role in the technologies to purify the polluted environment.

Brief Introduction to Catalytic Process

According to IUPAC, a catalyst is a substance that increases the rate of a reaction without altering the standard Gibbs energy change of a reaction. Catalysis can be of two types depending on the phase in which reactants and catalyst exists. If both reactant and catalyst exist in different phases, catalysis is known as heterogeneous catalysis. If not, it is homogenous catalysis. Most of the industrial processes are heterogeneous catalysis, which in general contains catalysts in solid phase and reactant in gas or liquid phase. Heterogeneous catalysts are more robust over a range of harsh reaction conditions. They are also separable making them prepared over homogeneous catalyst. The steps involved are adsorption, surface reaction and termination. Adsorption can be physisorption or chemisorption depending on the energetics of interaction between catalysts and reactant molecule. Physisorption is uneventful as far as reactions are concerned. Chemisorption of intermediate strength has relevance to catalysis.

On the surface of the catalyst, there are certain regions known as active sites, which directly participate in the reaction. They are usually under-coordinated surface atoms or defects, which can satisfy their coordination by bonding with the reactant molecule. This step is normally understood as chemisorption and invariably causes the activation of certain bonds on the reactant molecule. Activation of a molecule is understood in terms of weakening (or elongation) of the bonds that eventually breaks and combines with other reactants or surface adsorbed species to form new intermediates or products. Desorption of the newly formed product and regeneration of the active sites are crucial parts to complete a catalytic cycle. According to Sabatier's principle, the energy of interaction between the catalytic surface (adsorbent) and reactant (adsorbate) should be optimum for an eventful chemical reaction [4]. Number and nature of the active sites are critical parameters in evaluating catalytic performances, which are indicated by turn over numbers or frequency and selectivity of products. Catalysts are developed based on deep understanding of the chemical processes involved in the synthesis of the catalyst structure of active sites and energetics of the surface chemical reactions leading to products. Catalytic activity is also often found to be directly proportional to the surface area [5]. The process of heterogeneous catalysis relies on the adsorbate-adsorbent interactions, catalyst surface morphology, size of the particles, defects, etc.

Catalytic Oxidation Technology

In general, catalytic oxidation follows four steps. The first step is the adsorption step, where the reactant molecules (VOC/CO_x/NO_x) and oxygen adsorb onto the

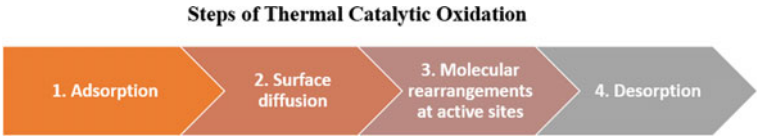

Fig. 13.2 Steps of thermal catalytic oxidation [6]

active sites of the catalyst. The second step involves the surface diffusion of atoms to adjacent adsorption/active sites. Molecular rearrangements or the reaction between oxygen and reactant molecule occur in the third step resulting in the oxidation products of the original reactant molecule. The last step is desorption of the products of the reaction from the surface of the catalyst [6] (Fig. 13.2).

There are three kinetic models proposed to explain the mechanisms of catalytic VOC oxidation. They are:

a. Langmuir–Hinshelwood (L–H) Mechanism: L–H mechanism proposes that both oxygen and the other reactant (e.g., VOCs) are adsorbed on to the surface and react to form the products (e.g., carbon dioxide and water). The rate determining step is the step in which reaction occurs between adsorbed oxygen and adsorbed reactant molecules. It can be of two types, single site and dual site based on same or different active site at which oxygen and reactant got absorbed.
b. Eley–Rideal (E–R) Mechanism: Either oxygen or reactant gets adsorbed onto the surface, which reacts with the molecule present in the atmosphere. So, the reaction occurs between either the adsorbed oxygen with reactants in air or between adsorbed reactants and oxygen in air which is the slowest step and hence the rate determining step.
c. Mars van Krevalan (MVK) Mechanism: According to the model, the reaction is triggered by the interaction of reactants and surface lattice oxygen in two consecutive steps. In the first step, the surface oxygen sites get reduced by reacting with reactant molecule and these sites will be regenerated either by the consumption of gaseous oxygen or by transfer of bulk oxygen to the surface in the second step [7] (Fig. 13.3).

Types of Catalysis Using Iron Oxides and General Materials Consideration

Depending on the nature of energy inputs, the reactive species might be different which can open a new reaction pathway on the surface of the catalyst. In the context of environmental catalysis, following types of catalytic reactions are known.

a. Photocatalysis: Photocatalysis is a catalytic oxidation of VOCs/NO_x/CO using a catalyst and light energy, particularly the visible region of the sunlight. Photocatalysts are mainly semiconductor nanoparticles with a specific band gap suitable enough to produce high energy excitons (photo-induced electron–hole pair) when light is shined on them. Absorption edge (λ_g) is related to the band gap (E_g) of the photocatalyst ($\lambda_g = 1240/E_g$). The photo-generated excitons can then produce reactive radicals, which can react with reactants such as VOCs to completely

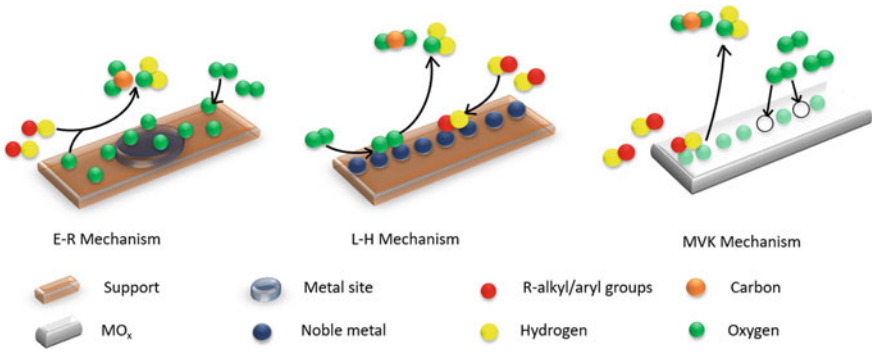

Fig. 13.3 Different mechanisms of thermal catalytic oxidation. Adapted from ref [7] with permission from Elsevier

oxidize them. Mitigation of reactants by photocatalysis is dependent on the quantity of photon flux available. On the other hand, deactivation of the catalysts is caused by surface contamination or aggregation of active sites. Photocatalysts are poised to treat the indoor pollution effectively when used in combination with construction materials such as window glasses, whereby visible spectrum of the sunlight or indoor light source can be utilized. A photocatalyst material that can efficiently utilize visible light without undergoing photo-induced damage is a challenge [8, 9].

b. Photothermal catalysis: Thermo-catalytic oxidation of reactants such as VOCs consumes relatively less energy compared to thermal oxidation. For the conventional photocatalysis, utilization efficiency of solar energy is small even after modification of the catalysts. In photo-thermo-catalysis, both thermal and photo processes are combined, whereby catalytic efficiency and durability of thermo-catalysis combined with low energy utilization of photocatalysis are expected to coexist. The thermal effects of vis-IR are utilized in photocatalysis to increase reaction efficiency or a broad range of solar spectrum is explored which simultaneously induces thermochemical and photochemical processes which synergistically catalyze the reaction [10] (Fig. 13.4).

It can be divided into two types based on the reaction pathway:

Photo-assisted thermal catalysis: Photothermal conversion can be defined as the conversion of sunlight into heat energy by collection and absorption system. Generally, there are three kinds of materials which can be used such as narrow band gap photocatalysts that can be excited by IR light, visible/near-IR plasmonic photocatalysts which carry out photochemical reactions by using plasmonic hot electrons, defective materials which can handle both light and heat like non-plasmonic oxide materials. Graphene is one of the materials which shows photothermal activity and some materials such as Mn-based catalysts doped with Fe, Cu and Mg [12]. Surface plasmon resonance effect is another process by which noble metals (Au, Ag and Pt)

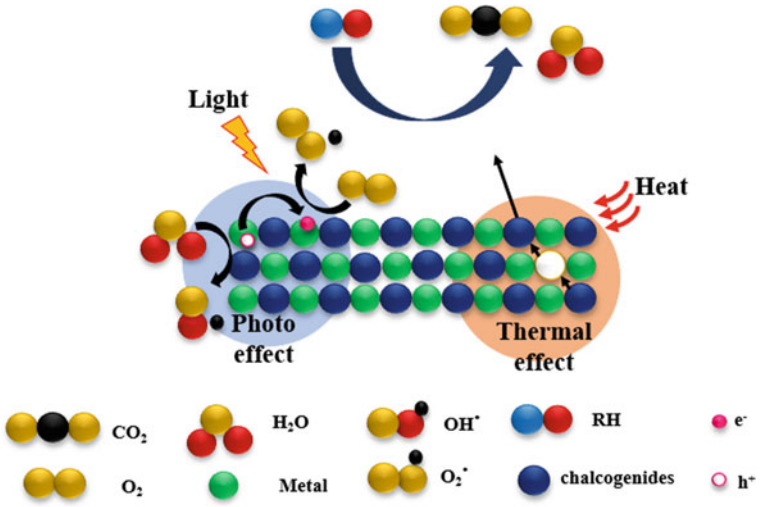

Fig. 13.4 Diagram representing photo-thermal catalysis Adapted from ref [11] with permission from Wiley VCH GmbH

absorb light and scatter it. Incorporating these metals into the catalyst will improve light harvesting ability hence the photo-thermo catalytic activity.

Photo-thermal synergistic catalysis: The advantages of both thermal catalysis and photocatalysis are combined to have the synergistic effect, which enhances the catalytic performance. A semiconductor material with narrow band gap usually shows excellent performance [13].

c. Plasma catalysis: When a gas is exposed to an electric field of desired magnitude, it will get ionized to ions and electrons. The partially ionized gas with electrons, ions and neutral species interacts with each other giving rise to reactive environment called plasma. In plasma catalysis, both plasma and catalyst enhance the reaction rate independently and inter dependably. Plasma initiates a few processes on the surface such as sputtering, [14] etching [15, 16] formation of hotspots and charging. The interdependence of plasma and catalysts known as synergistic behavior, which improves energy efficiency, conversion percentile and selectivity for the reaction. At the plasma catalyst interface, plasma establishes an electric field and changes the gas composition by producing reactive species, ions, electrons and photons to the surface, whereas catalyst lowers activation energy for some reactions. At the interdependent state, plasma alters the surface morphology or work function of the catalyst and dielectric constant, or morphology of the catalyst affect energy distribution in plasma. Vibrationally excited species are important because they influence plasma surface interactions more. Generally, for a nanoparticle to be active, the requirements are size, faceting, uncoordinated surface atoms and other defects, active sites, strain, oxidation state, charge transfer, etc. During plasma catalysis, all these factors will be modified by plasma

thus effecting the catalytic activity. The requirements of a material to be tried for plasma catalysis can be summarized as having a large contact area for strong interaction and a higher dielectric constant of the catalyst. A shorter distance between plasma and catalyst facilitates the reaction of the short-lived radicals to the maximum. Most of the active catalysts are transition metals [17]. Plasma catalysis not only prevents coke formation and catalytic poisoning which are inevitable in thermal catalysis but synergism in plasma catalysis even modifies the reaction pathway (Fig. 13.5).

Synthesis of Iron Oxide-Based Catalysts

Proper identification of experimental conditions for the preparation of catalysts is extremely important for the activity of nanoparticles [2]. Iron oxide nanoparticles and nanocrystals are considered as 0 D architectures of iron oxide, used mostly for biomedical and catalytic applications. Desirable features of nanoparticles like narrow particle size distribution, good dispersion and stability can be achieved by optimizing reaction conditions like choice of iron precursor, solvent, concentration of reducing agent, pH, reaction temperature and time. Co-precipitation is often used to prepare iron oxide nanoparticles in water which involves adding a base to the precursor solution which contains Fe(II) or Fe(III) ions to promote the precipitation of ferrihydrites and subsequent dehydration generates iron oxide nanoparticles. Employing different

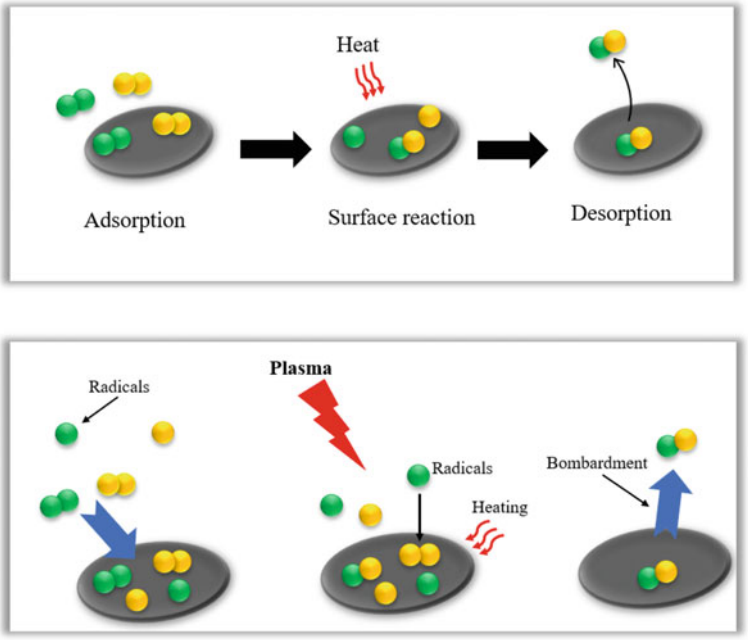

Fig. 13.5 Diagram differentiating thermal and plasma catalysis [17]

bases, ionic medium, pH and iron precursors the formation of desired phase of iron oxide can be achieved [18]. Solvothermal methods have the added advantages of being low cost, high yield and greater control over the phases and requirement of moderate temperature. In a typical solvothermal synthesis by adjusting concentrations of ferrous chloride and ratio of ethanol/water mixture, particle size can be tuned from 15 to 31 nm. Higher particle concentrations of $FeCl_2$ create more nuclei and finally to smaller particles and more the amount of ethanol in the solvent also created smaller particles by inhibiting the particle growth [19].

13.2 Catalytic Oxidation of VOCs by Iron Oxide-Based Catalysts

Air pollutants are mainly of two types: *Particulate pollutants, which can be removed by adsorption techniques,* and *Gaseous pollutants* (in sub ppm levels), which consists of VOCs as a major share. Among them, VOCs are not easily removable and their mitigation has been under the special focus for several years. The European Union defines any organic compound having an initial boiling point $\leq$ 250 °C measured at standard atmospheric pressure of 101.3 kPa as VOCs. They are acknowledged as hazardous to human health as well as to the environment mainly because of its high volatility, persistence in the environment, ability to spread over long distances from the point of release and ability to get transformed to other hazardous compounds by chemical reactions, often under normal atmospheric conditions. In India, the Clean Air Act 1990 (Amendment) and the Factory Act 1986 (Amendment) limit the emission of hazardous chemicals including VOCs [20]. Due to the current scenario of strict regulations on the concentration of VOCs in indoor as well as outdoor environment, either recovery techniques or oxidative techniques are applied. Recovery techniques involve both separation of the VOCs and particulate matter from the air followed by its recovery from the adsorbents. Adsorption, membrane separation and condensation methods come under the category of recovery techniques. Adsorption method is suitable only for dilute VOC emissions like the removal of solvent vapors in the atmosphere. Membrane separation and absorption methods are expensive because of the maintenance of the setup. Condensation is useful for VOCs with higher boiling points where the oversaturation is achieved by cooling or pressurizing the gas stream. The major disadvantage associated with these methods includes the lack of solutions to dispose of the VOCs recovered from the adsorbent. On the other hand, oxidative techniques involve the complete oxidation of the VOCs into carbon dioxide and water. Thermal incineration is a viable alternative despite being highly energy-demanding. The important disadvantage of the incineration method is the production of incompletely oxidized volatile byproducts, which invariably happens. This certainly aggravates air pollution instead of mitigating it. Hence, catalytic oxidation is a very powerful technology to completely oxidize the volatiles to relatively harmless carbon dioxide and H_2O at reasonable temperatures.

Belessi et al. carried out kinetic studies of the deep oxidation of CH_4 on oxide solids $La_{0.7}Ce_{0.3}FeO_3$, $La_{0.7}Sr_{0.3}FeO_3$, $La_{0.7}Sr_{0.1}Ce_{0.2}FeO_3$ oxide solids having mixed oxide and perovskite phases. From the kinetic analyses of the reaction rate, it is found that adsorbed oxygen in dissociative form reacted with gaseous methane, following the Eley–Rideal model. The existence of a $SrFeO_{3\pm x}$ perovskite crystal phase, which can uptake large amounts of oxygen accounts for the large value of heat of adsorption of oxygen, $\lambda_{O_2} = 53–211$ KJmol^{-1} [21].

Catalytic oxidation of VOCs by Fe-based materials using thermal, photo, photothermal, and plasma techniques is summarized in Tables 13.1, 13.2 and 13.3. Low-temperature catalytic activity is shown by Fe–Ce mixed oxides on SBA-15(Sl no 4) hence even better than supported Au catalyst (SI no 32). The higher activity can be due to the better dispersion of metal oxides over the porous structure of the material. Higher conversion with lower specific input energy (SEI = plasma power (kW)/flow rate(*L*/min)*X* 60 s/min) was shown by Fe-doped Mn octahedral sieves. Modifying defects and surface area of the catalysts by various methods improved the production of active species in plasma and oxygen mobility on the surface to enhance the mitigation efficiency of the catalysts for various VOC oxidation. Generally, iron oxides show good activity among the other oxides in the oxidation of chlorinated VOCs with the added advantages of high efficiency, low cost and environmental friendliness. Recently, studies were carried out with Fe–Mn mixed oxides for the oxidation of toluene, formaldehyde, chlorobenzene and dichlorobenzene [23, 58]. Among those, chlorinated VOCs are more important because of their contributions to the production of secondary organic aerosols, peroxyacetyl nitrate, tropospheric ozone and the greenhouse effect. Noble metal catalysts have the disadvantage of chlorinated compounds due to deactivation by HCl, Cl_2 poisoning and chlorination of products other than oxidation [22]. Ru is known to be resistant to Cl poisoning by promoting deacon reaction. It is known that supports do affect the catalytic activity by altering the crystallite dimensions and thermal stability of the metal species. Wang et al. studied the possible application of Ru doped on mesostructured Fe–Mn oxides. The mesoporous Fe–Mn bimetallic oxide with a metal atomic ratio of 1:2 was prepared by oxalate pyrolysis without any template followed by metal impregnation for doping with Ru. The XRD data did not show any active phases of Ru and no significant diffraction peaks of Mn which means that the active phase of Ru is stabilized in the mesoporous substrate by strong metal-support interactions [23]. In a recent study by Fan et al., HCHO oxidation was carried out using Fe–Ce–O catalyst supported on mesoporous silica prepared by simple impregnation-calcination resulting in the formation of small solid solution particles with good dispersion in confined spaces. CeO_2 materials are routinely investigated along with other transition metal oxides for VOC oxidation but suffer from having a low surface area and limited efficacy for low-temperature oxidation. Many methods were explored to lower the activation barrier such as doping other metal atoms and creating more oxygen vacancies. Activity achieved at a low temperature of 60 °C was associated with the presence of Fe content which along with the calcination temperature influenced the activity by increasing oxygen vacancy [25]. Xiaodong et al. tried mesoporous Ti-doped iron oxide for the degradation of ortho-dichlorobenzene. Surprisingly, the Ti-doped iron

oxide was showing better activity compared to the individual counterparts, which can be due to the presence of Ti^{4+} which had a higher affinity toward chlorinated VOCs, and iron oxide which showed a better oxidation power. It has also been proven that TiO_2 alone has a slower activity which proves the active component is iron oxide. The study mostly concentrates on regulating the composition and hence the structure of the TiO_2–Fe_2O_3 system to gain more knowledge about the interface interactions between both. It was prepared by CTAB as the structure-directing agent [22]. For example, Bismuth ferrite with a rhombohedrally distorted perovskite structure is a multiferroic compound that exhibits ferroelectricity and weak ferromagnetism above room temperature. Due to the narrow band gap energy (2.2 eV) and excellent chemical stability, these materials have applications in visible light photocatalysis. However, the electrical and multiferroic potential applications of BFO magnetic nanoparticles are hindered due to the following properties such as weak ferroelectricity, remanent polarization, high leakage current density, poor ferroelectric reliability and inhomogeneous weak magnetization. The substitution of any of the A-site and B-site had significant improvement in the multiferroic and photocatalytic properties [60].

Materials Consideration for Heterogeneous Catalysts for VOC Oxidation

If the VOC is an *N*-containing one, then there is a chance for the generation of nitrogen oxides, and if it is *S*-containing, the formation of metal sulfates is inevitable and which leads to the deactivation of catalysts. The key step for catalytic oxidation is the adsorption of the compound onto the surface of the catalyst with subsequent activation. In activating oxygenated VOCs, the abundance of OH groups on the surface plays a significant role. Introducing alkali metal salts onto the supported metal increases the concentration of –OH groups. For example, using noble metal catalysts for chlorinated VOCs has the disadvantage of easy deactivation as well as generating polychlorinated pollutants as byproducts. Even though increasing the acidity of the support decreases the selectivity toward polychlorinated byproducts, the application of noble metal catalysts for chlorinated VOCs is not advisable. Hence, selecting a catalyst also depends on the functional groups present, and in the case of a mixture of compounds, the mutual chemical interaction plays a crucial role in the choice of metal, support, precursor, preparation method, reaction conditions and catalytic reactor to be chosen. Hence, designing new catalysts which are active at low temperatures with high selectivity and low cost is critically important in practical applications.

Supported Noble Metal Catalysts (SNMCs) and Transition Metal Oxides (TMOs) are in general used as catalysts where the former have superior activity, selectivity and ease of regeneration despite being costly. So, the noble metal atoms are dispersed on a support which can be simple oxides such as silica or alumina, transition metal oxides or molecular sieves. Based on the involvement in chemical transformation, supports are classified into active or inert. Active support gets involved in catalytic oxidation, whereas inert support does not show any catalytic activity but provides surface and pore structure for the uniform dispersion of active metal catalysts. The presence of these supports not only reduces the amount of noble metal used, which is an economical advantage but also increases the dispersion of active sites thereby

Table 13.1 Catalysts for VOC oxidation by thermal catalysis

S. No.	Catalyst	VOC	T (K)	Conversion (%)	References
1	Ti-doped iron oxide	1,2-Dichlorobenzene	623	100	[22]
2	Ru-doped porous Fe–Mn oxide	Chlorobenzene	470	90	[23]
3	PtPdFe nanoparticle	Propene	383	50	[24]
4	Fe-Ce mixed oxide supported on SBA-15	Formaldehyde	333	100	[25]
5	Mn incorporated mesoporous ferrihydrite	Acetaldehyde and toluene	353	99	[26]
6	Fe zeolites	Toluene and ethanol	649 (Toluene) and 530 (Ethanol)	98	[27]
7	Ce_{1-x} $Fe_xO_{2-\delta}$	Methane	773	100	[28]
8	Iron molybdate	Methanol	503	100	[29]
9	Fe/SBA-15	Methane thiol	713	100	[30]
10	Co–Fe layered double oxide/Fe mesh	Toluene	620	90	[31]
11	$Au/FeO_x/CeO_x$	Methanol and toluene	433 (Methanol) and 583 (Toluene)	100	[32]
12	Fe/MnO_x	1-Methoxy-2-propyl acetate	533	100	[33]
13	Iron titanate	Chlorobenzene	573	100	[34]
14	Pt/Iron oxide	Xylene	498	100	[35]
15	Fe(III) intercalated titanium phosphate	Acetone, methanol and diethyl ether	483 (Acetone), 533 (Methanol), 543 (Diethyl ether)	100	[36]
16	Ferric sludge	Propane and toluene	633 (Propane) and 493 (Toluene)	100	[37]
17	MnO_2 decorated $Co_3Fe_1O_x$	Toluene	516	90	[38]
18	Iron–titanium–hafnium oxide	Ethyl acetate	700	100	[39]

(continued)

Table 13.1 (continued)

S. No.	Catalyst	VOC	T (K)	Conversion (%)	References
19	Fe-pillared montmorillonite	Toluene and chlorobenzene	673 (Toluene) and 723 (Chloro benzene)	100	[40]
20	Fe–Mn mixed oxides	Ethanol, ethyl acetate and toluene	492 (Ethanol), 518 (Ethyl acetate) and 566 (Toluene)	80	[41]
21	Iron oxide impregnated on clay	Toluene	623	100	[42]
22	$0.25Pt_1/meso\text{-}Fe_2O_3$	Benzene	471	90	[43]
23	Au/Fe_2O_3	Isopropanol, ethanol, acetone and toluene	473(Methanol), 523(Ethanol) and 473(Isopropanol)	100	[44]
24	Fe_2O_3	Chlorobenzene	673	90	[45]
25	Fe-Ti binary oxides	Ethyl acetate	725	100	[46]
26	Fe–Mn mixed metal oxides	Chlorobenzene	470	90	[47]
27	Mesoporous Fe_2O_3	Acetone and methanol	462 (Acetone) and 481 (Methanol)	90	[48]
28	MnFe mixed oxide	Ethanol and propane	493 (Ethanol) and 623 (Propane)	100	[49]
29	Co-Fe spinel oxide	Ethanol	548	100	[50]
30	$Cu_yCo_{3-y}FeO_x$	Toluene	523	100	[51]
31	Cu-oxo-Fe/silica	Toluene	723	80	[52]
32	$Au/\alpha\text{-}Fe_2O_3$	Formaldehyde	343	100	[53]
33	Iron oxide/porous clay heterostructures	Toluene	471	90	[54]
34	Fe–Mn mixed oxides	1,2-Di chlorobenzene	673	100	[55]
35	Mn–Fe binary oxides	Toluene	443	100	[56]
36	Fe/TiO_2-pillared montmorillonite	Toluene	648	100	[57]

Table 13.2 Catalysts for VOC oxidation by photo and photothermal catalysis

Sl No	Catalyst	VOC	Conversion (%)	Experimental conditions	References
1	Fe-doped MCM-41	Trichloroethylene	90	365 nm	[58]
2	Fe/TiO_2	Acetaldehyde	90	White light	[59]
3	Ba-doped $BiFeO_3$	Benzene and toluene	81% (Benzene) and 91% (Toluene)	Visible light 50 min irradiation	[60]
4	Au/Fe_2O_3	Formaldehyde	30	Blue light	[61]
5	Iron oxide micropine dendrites	Toluene	55	150W Xe lamp, 200 min irradiation	[62]
6	Mesoporous $ZnFe_2O_4$	Benzene	60	60 W tungsten lamp, 30 min irradiation	[63]
7	Fe-doped TiO_2	Acetaldehyde	100	Visible light, 500 min irradiation	[64]
8	Graphene/ Fe^{3+}–TiO_2	Formaldehyde	58	–	[65]
9	N-doped graphene/ Fe_2O_3	Acetaldehyde	55	–	[66]
10	Mesoporous amorphous Mn–Fe oxide	Benzene	90% at 287	$\lambda > 420$ nm Vis-IR and $\lambda > 830$ nm IR irradiation	[12]

Table 13.3 Catalysts for VOC oxidation by plasma catalysis

Sl No	Catalyst	VOC	Conversion (%)	Specific input energy (J/l)	References
1	Fe_2O_3/sepiolite	Toluene	90	550	[67]
2	Fe/cordierite	Diethyl ether	95	600	[68]
3	Fe-doped manganese oxide octahedral molecular sieves	Trichloroethylene	90	130	[69]
4	$LaFeO_3$	Ethyl acetate	85	600	[70]
5	Fe_x-Mn_y/Al_2O_3	Toluene	100	1500	[71]
6	ZrMnFe/Sepiolite	Toluene	95	950	[72]

increasing the number of molecules interacting with the active site. In addition, the acid–base properties of support help in more dispersion of noble metal over the catalyst. Despite being less active, TMOs are good alternatives to SNMCs due to low cost, reducibility and thermal stability, and most importantly resistance to poisoning which is most common with noble metal catalysts. The activity of a catalyst or the reaction rate of the oxidation mainly depends on physical and chemical properties as well as the morphologies of active metal and support.

13.3 CO Oxidation

CO is a gaseous air pollutant produced due to the incomplete combustion of fuels from automobiles, industrial processes and power generation. Indoor sources include leaking chimneys, unvented kerosene and gas space heaters and gas stoves. At very high concentrations in indoor or enclosed environments, CO causes dizziness, confusion, unconsciousness or even death. CO is a colorless and odorless gas and can irreversibly bind with haemoglobin causing depletion in the oxygen levels in cells, which ultimately leads to cell death. CO is aptly described as a "silent killer". Developing an efficient catalytic oxidation system for CO is highly desired, not only because it is poisonous but its industrial significance in the synthesis of methanol and other fuel and pure hydrogen in proton membrane exchange fuel cells [73].

The state-of-the-art catalysts for CO oxidation are noble metals but their use is limited because of high cost, low abundance and poisoning. High dissociation probability, low adsorption energy due to the half-filled d-bands and low cost have made TMOs as an attractive alternative [73]. SNMCs are also actively pursued as it shows increased exposure of active sites and decreases the consumption of expensive metal component. Bimetallics of noble metals with transition metals such as Mn, Fe, Co, Ni and Cu retain the superior catalytic property of the noble metals at a lower cost. Au is the most investigated noble metal catalyst due to the presence of Lewis acid sites, ease of size and shape [2]. In SNMCs, the nature of the support plays an important role since the reaction either takes place at the interface of the metal and the oxide support or as a spillover of reactive species from or into the oxide layer. Also, semiconductor metal oxides like TiO_2, Fe_2O_3 and NiO form more stable catalysts than insulating metal oxides such as Al_2O_3 and SiO_2. The Turnover Frequency (TOF) of Au catalysts changes significantly compared to Pt with the preparation method. The table given below indicates clearly that contact structure determines activity in supported Au catalysts [74] (Table 13.4).

In general, Strong Metal Support Interaction (SMSI) can be explained as the change in catalytic reactivity of reducible oxides supported by group VIII metals after the high-temperature reduction process. Au particles supported on reducible oxides such as TiO_2, Fe_2O_3 and CeO_2 possess improved oxidation activity compared to unsupported ones. SMSI induces both electronic and geometric effects on the catalyst and it can be strong or weak. Contact at the interface induces electronic redistributions leading to the formation of a new phase at the metal-support interface

Table 13.4 Comparison of the activity of Au and Pt-supported catalysts for CO oxidation [74]

Metal	Preparation method	Diameter of the particle (nm)	$T_{50\%}$ (K)	TOF at 300 K (s^{-1})
Pt	Deposition	1.3	334	2.7×10^{-3}
	Impregnation	1.4	339	3.8×10^{-3}
	Phase distortion	2.4	363	9.2×10^{-3}
Au	Deposition	3.1	282	3.4×10^{-2}
	Deposition	2.7	253	1.2×10^{-1}
	Impregnation	10	481	–
	Phase distortion	4.6	477	9.6×10^{-6}

[75]. As a geometric effect, metals supported on reducible oxides exhibit SMSI, which is the encapsulation of metal by a thin layer from the oxide support. It is shown that Pt supported on Fe_2O_3 (111) also exhibits SMSI via encapsulation due to the strong adhesion energies between Pt and iron oxide. Pt particles heated above 800 K in a vacuum exhibit structure that is like ultrathin FeO (111) film on Pt (111) single crystal. The catalyst showed higher activity compared to Pt (111) surface which is explained due to the formation of inverted catalysts or highly dispersed FeO_x nanoparticles on the Pt (111) surface [76] (Fig. 13.6).

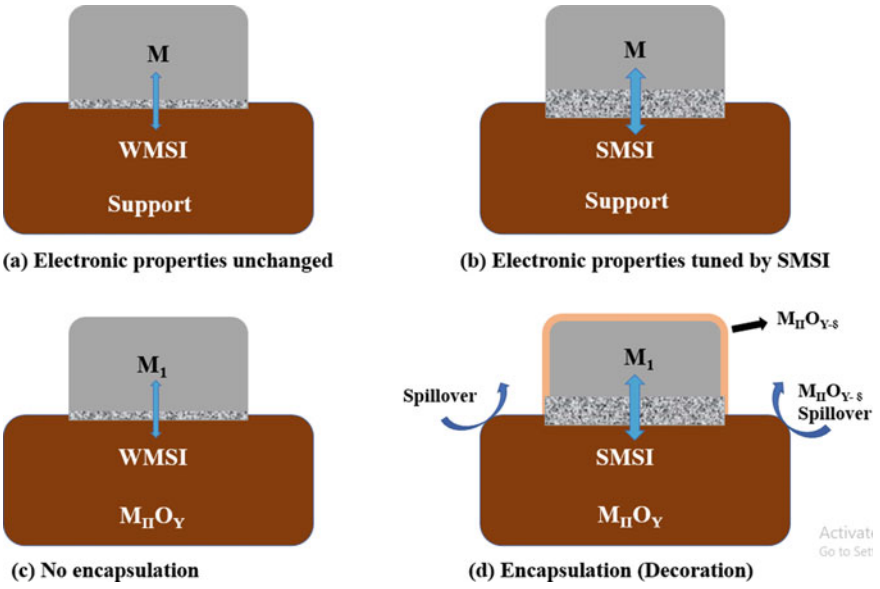

Fig. 13.6 Diagram showing electronic effects (**a**, **b**) and geometric effects (**c**, **d**) of SMSI Adapted from ref [75] with permission from Elsevier

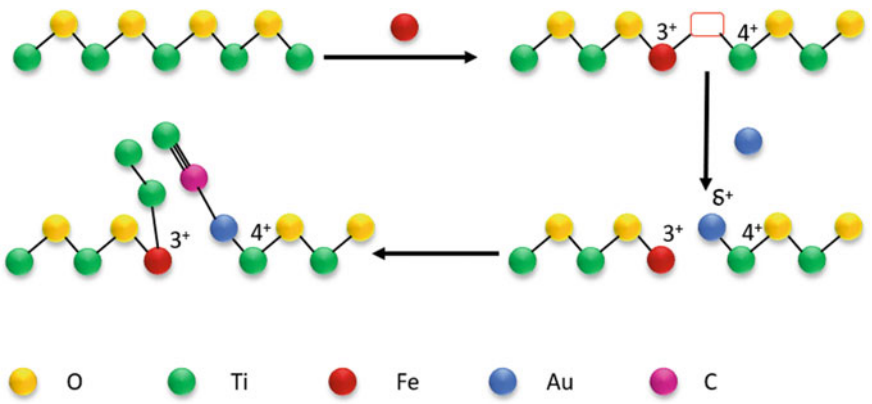

Fig. 13.7 Mechanism of CO oxidation over Fe-doped TiO_2 Adapted from ref [77] with permission from Wiley VCH GmbH

A significant number of studies on low-temperature CO oxidation catalysts are based on Au nanoparticles supported on iron oxide. Since the oxidation reaction occurs at the interface of Au nanoparticles and support, several factors like the size of the Au particle, the nature of support and the contact structure between support and Au were reported [74] to be controlling the catalytic activity. Cui et al. reported that increasing the pH value during synthesis is proportional to the catalytic activity due to stronger interaction between Au–OH–Fe or Au–Fe–O structure. They also found that calcination temperatures above 673 K eliminated surface hydroxyl groups which resulted in lower catalytic activity [2]. Oxidation of CO on iron oxides can occur in presence of oxygen and it is considered to proceed through dissociative adsorption of oxygen and removal of oxygen by CO through an Eley–Rideal mechanism [76]. Given below is a schematic representation of CO oxidation catalyzed by Au supported on Fe-doped TiO_2 which clearly indicates that Fe catalyzes the dissociation of oxygen molecules [77] (Fig. 13.7, Table 13.5).

Iron oxide-based catalysts tested for CO oxidation along with the temperature and conversion are given below as a table. Complete conversion of CO at lower temperatures is exhibited by catalysts with noble metals. Besides, the activity of the supported catalysts is in the order of Au > Pt > Pd. Particularly, among transition metal oxide catalysts, good activity was observed when iron was combined with Cu followed by Co. When iron oxide is used as the support, geometric and electronic effects of SMSI improve the catalytic activity.

Table 13.5 Comparison of activity of catalysts for CO oxidation

S. no	Catalyst	T (K)	Conversion (%)	References
1	$Ce_{1-x}Fe_xO_{2-\delta}$	673	100	[28]
2	Fe–Co mixed oxide	423	100	[78]
3	$LaFeO_3$	914	90	[79]
4	PtCu/ɣ-Fe_2O_3	298	100	[80]
5	Pt/exsolved FeOx/$LaFeO_3$	296	100	[81]
6	Au/Fe_2O_3	263	50	[82]
7	CuO/Fe_2O_3	373	100	[83]
8	10% CuO/α-Fe_2O_3 nanorods	373	100	[84]
9	Fe–Co mixed metal oxide	473	100	[85]
10	Pt/FeO_x	296	100	[86]
11	Pd/FeO_x	475	100	[87]
12	Fe_2O_3	573	100	[88]
13	CuO-doped $Fe_4Ti_{10}Sn_{10}$ composite oxides	423	100	[89]
14	Fe, Ce and Al pillared bentonite	573	100	[90]
15	Au/Fe_2O_3	398	100	[91]
16	Au/$FeTiO_2$–Fe	363	100	[92]

13.4 Selective Catalytic Reduction (SCR) of NO*x*

Nitrogen oxides (NO, NO_2, and their derivatives), in general, denoted as NO_x is a gaseous pollutant that can cause photochemical smog, acid rain and ozone depletion leading to global warming and eutrophication problems. Major sources are automobiles and other industries and there are regulations for power plants and engines regarding emissions. According to the United States Environmental Protection Agency, the NO_x emission of an engine should be within the limit of 0.02–0.10 g/bhp-hr. Amount of NO_x and VOCs is responsible for the presence of hydroxyl radicals hence the oxidizing ability of the stratosphere. In urban areas where a high concentration of NO_x is present, it controls radical production hence the oxidizing ability, and in rural areas with relatively low concentrations of NO_x VOCs control the radical production. The reaction of NO with VOCs which is responsible for the photochemical smog is shown below (Fig. 13.8).

Photochemical smog is brown in color and affects the throat, causes chest pain, the difficulty of breathing for humans, cracking of rubber and damages plant life too. Hence, reducing and mitigating NO_x is important.

SCR of NO by NH_3 is widely used for removing NO from the atmosphere. In SCR, NO_x is converted to dinitrogen and water in the presence of a catalyst as well as a reducing agent. Commonly used reducing agents are anhydrous or aqueous ammonia or urea solution which is added to the stream of gas which flows through the catalyst. Commercially used catalytic systems for SCR reactions are V_2O_5–MoO_3/TiO_2 and

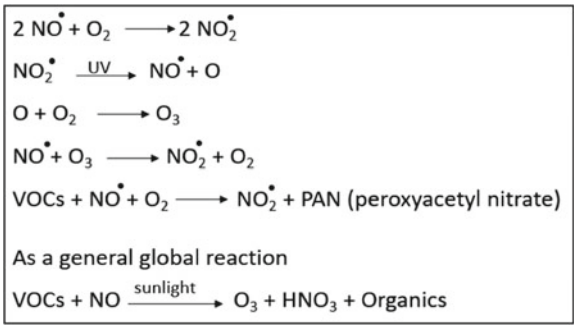

Fig. 13.8 Reaction of NO with VOCs generating photochemical smog [93]

V_2O_5–WO_3/TiO_2 [94, 95]. The commercial system has some drawbacks such as a reduction in the selectivity of N_2 in the temperature range of 573–673 K, the need to reheat the stack gas, sulfur poisoning and the toxicity of vanadium pentoxide [96–98]. TMOs are investigated the most due to the easy gain and loss of *d* electrons, low cost and stability [99]. A few Fe-based catalysts that showed good conversion in the low-temperature range were Fe–MnO_x and Fe_xTiO_y [100, 101]. Mn is explored extensively due to the variable oxidation states and redox stability hence the activity at the lowest temperature. But the drawback of Mn is with low selectivity of N_2 and sensitivity toward SO_2 in the gas flow [102–104]. Due to the environment-friendly nature and low cost, easy reducibility and mobility of active surface oxygen, iron oxides have also been explored nowadays either in combination with other transition metals or as support with other elements [100, 105]. The drawback associated with iron oxide is low surface acidity, low N_2 selectivity above 623 K and low resistance to SO_2 and H_2O.

Mechanism of SCR with NH_3

The possible mechanism for SCR of NO in presence of NH_3 catalyzed by $Mn_2O_3^-$ Doped Fe_2O_3 is shown in Fig. 13.9. Four types of species are indicated by DRIFTS spectra after the adsorption of NO on the catalyst, they are gaseous NO_2, bidentate nitrates, linear nitrites and monodentate nitrites. Adsorbed NH_4^+ ions combine with NO_2^- to form NH_4NO_2. Fe and Mn are involved in a redox cycle to continue the reaction, while NH_3 acts as the hydrogen source for the reduction. After each cycle, Fe^{3+} is regenerated by Mn^{4+}. Mn^{2+} is again oxidized by oxygen to continue the cycle of reaction.

Different catalytic systems involving iron as a dopant or support, the temperature of SCR and the percentage conversion are given in Table 13.6. Fe–Mn system is investigated the most and it shows the maximum activity at the lowest possible temperature. Activity at the lowest temperature is exhibited by porous MnO_x–FeO_x nanoneedles (Sl no 3) which can be due to the uniform distribution of the ions, availability of redox sites, porous structure and strong acidic sites. Various catalysts were tried for the NH_3-catalyzed SCR reaction. It has been observed that the modified catalyst exhibits improved activity over the commercial catalysts known and have good selectivity toward nitrogen.

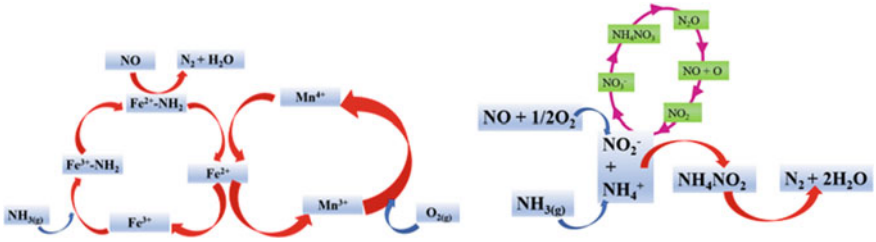

Fig. 13.9 Mechanism of SCR with NH_3 in presence of $Mn_2O_3^-$ doped Fe_2O_3 hexagonal microsheets. Adapted from ref [106, 107] with permission from Elsevier and American Chemical Society

Table 13.6 Comparison of activity of catalysts for SCR reaction

Sl No	Catalyst	T (K)	Conversion (%)	References
1	Mn_2O_3-doped Fe_2O_3 hexagonal microsheets	473	98	[106]
2	MnO_x supported on Fe–Ti spinel	448	100	[107]
3	Porous MnO_x–FeO_x nanoneedles	393	100	[108]
4	MnO_2-doped Fe_2O_3 hollow nanofibers	423	98	[109]
5	Fe–W mixed oxide	523	100	[105]
6	$MnFeO_x$ nanorods	473	98	[110]
7	Dy-doped $MnFeO_x$ nanowires	423	100	[111]
8	Co–Fe mixed oxide	443	100	[112]
9	$Fe_9Ti_1O_x$	523	80	[113]
10	WO_3–FeO_x	523	98	[114]
11	12-tungsto phosphoric acid/iron oxide	523	100	[115]
12	Mn–Fe oxides on Fe mesh	453	98	[116]
13	Fe-modified MnO_2	523	75	[117]
14	$MnFeO_x$/CNT	413	100	[118]
15	Mesoporous Mn–Fe Spinel	398	100	[119]

13.5 Fenton Reaction

The Fenton process was developed in 1894 by a French scientist Henry J Fenton who discovered that at pH 2–3, tartaric acid can be oxidized by the Fe^{2+}/H_2O_2 system. Fenton's process comes under the category of Advanced Oxidation Processes (AOP). The importance of this process is that toxic organic pollutants cannot be easily removed by conventional wastewater treatment processes and the abundant availability of resources such as iron and H_2O_2. Depending on the number of phases involved in the reaction, it can be classified into a homogenous Fenton process where only a single phase is involved and a heterogenous Fenton process where dual phases are present. The classical reaction is a homogenous Fenton process with Fe^{2+}

interacting with H_2O_2 in the solution state. In the presence of H_2O_2, which acts as an oxidizing agent, ferrous ions (Fe^{2+}) are converted to ferric ions (Fe^{3+}) (Eq. 13.1). This oxidation is the first step in Fenton's reaction. This results in the formation of a hydroxide ion (OH^-) and a hydroxyl radical (·HO) as byproducts. To continue the activation of H_2O_2, Fe^{2+} can be obtained via the reduction of Fe^{3+} by H_2O_2 (Eq. 13.2). The reduction of Fe^{3+} is very slow and generates hydroperoxyl radicals ($HO_2^{\cdot}$) which has a weaker oxidation ability than ·HO. Two different oxygen free radicals are formed when hydrogen peroxide molecules undergo disproportionation (Eq. 13.3). The produced hydroxide ions and protons combine to form water (Eq. 13.4).

$$Fe^{2+} + H_2O_2 \rightarrow Fe^{3+} + OH^- + \cdot HO \tag{13.1}$$

$$Fe^{3+} + H_2O_2 \rightarrow HO_2^{\cdot} + Fe^{2+} + H^+ \tag{13.2}$$

$$2H_2O_2 \rightarrow HO_2^{\cdot} + {}^{\cdot}HO + H_2O \tag{13.3}$$

$$Fe^{2+} + H_2O_2 + H^+ \rightarrow Fe^{3+} + {}^{\cdot}HO + H_2O \tag{13.4}$$

To improve the efficiency of the process, Fenton's process is often coupled with electro/UV/sono such as to increase the amount of ·HO and the regeneration of Fe^{2+} to Fe^{3+} [120]. Even then there are some disadvantages associated with the process. A continuous supply of H_2O_2 is required which makes the process economically non-viable and the formation of solid ferric sludge needs to be removed periodically along with the loss of iron ions. Overall, the process becomes expensive [121–123]. Increased production of reactive oxygen species was observed in hybrid systems where two of the modified Fenton process were combined like in Photo-Electro-Fenton (PEF). Even though an enhancement in activity is observed, compared with the real situation of huge amounts of wastewater reduced chemical consumption cannot be equated to electricity loss. Considering the example of the electro-Fenton process even though the process efficiency is higher, Fe is getting consumed at the anode. Recovery and reuse of iron sludge in this context may be addressed by using acid treatments and ion exchange. Ferrites thus prepared were again employed in the process.

Introducing iron in the heterogeneous solid phase has proved to be safe, efficient and cost-effective. Homogenous and heterogeneous Fenton processes differ in the fact that in heterogenous Fenton, ·HO production occurs on the surface of the catalyst, and also the reactant molecules get adsorbed on the active sites and after the reaction, they get desorbed and active sites are free for the next cycle [124, 125].

$$X - Fe^{2+} + H_2O_2 \rightarrow X - Fe^{3+} + \cdot OH + OH^- \tag{13.5}$$

$$Fe^{3+} + H_2O_2 \rightarrow X - Fe^{2+} + \cdot O_2H + H^+ \tag{13.6}$$

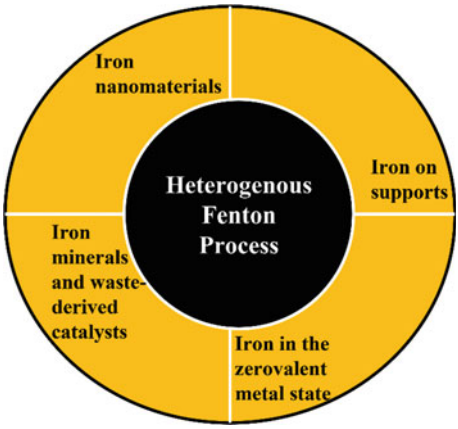

Fig. 13.10 Forms of iron catalysts employed for heterogenous Fenton process

Table 13.7 Iron-based heterogeneous catalysts used for the degradation of various pollutants

Sl No	Catalyst	Pollutant	Removal efficiency (%)	References
1	Magnetite	Reactive blue 19	87	[130]
2	Magnetite	Acid red 18	83	[131]
3	Haematite	Acid red 18	81.5	[131]
4	Iron molybdophosphate	Landfill lechate	82	[132]
5	Pd/Fe_3O_4	Humic acid	90	[133]
6	Chalcopyrite	Tetracycline	99	[134]
7	Pyrite	Levofloxacin	95	[135]

Reaction rate increases with higher surface area and porosity as usual with general catalysts are observed here too [126].

Advantages of heterogenous Fenton process [127–129] (Fig. 13.10, Table 13.7).

- Operating under a wide temperature range
- Zero formation of iron sludge hence reducing additional removal costs
- Easy handling and safe storage
- Easy recovery by sedimentation, filtration and magnetic separation

13.6 Conclusion

Mitigation of environmental pollutants by catalytic technology is one of the promising areas of research that can directly address the goals set by the UN and other international agreements. Particularly, the literature suggests that iron and iron oxide-based catalysts or supports have been extensively tested due to their intrinsic activity or promotional activity as support, high natural abundance, low cost and no

toxicity. The chapter discussed iron oxide applied in four environmentally important reactions such as VOC oxidation, CO oxidation, SCR reaction of NO_x, and Fenton reaction. After comparing the catalytic activity, it can be understood that Fe plays a significant part in improving the catalytic activity. Although the major challenges with respect to activity and selectivity remain to be addressed. It is however possible that economically viable large-scale catalytic processes are likely to contain iron in their composition.

Acknowledgements The authors thank IIT Palakkad for the infrastructure and support. The author S. Anaina 2nd year BS–MS student from IISER Berhampur worked as an intern for two months in the group of Dr. Dinesh Jagadeesan at IIT Palakkad.

References

1. Cornell RM, Schwertmann U (2003) The iron oxides: structure, properties, reactions, occurrences, and uses, vol 2. Wiley-vch, Weinheim
2. Tanaka S, Kaneti YV, Septiani NLW, Dou SX, Bando Y, Hossain SA, Kim J, Yamauchi Y (2019) A review on iron oxide-based nanoarchitectures for biomedical, energy storage, and environmental applications. Small Methods 1800512:1–44
3. Kankaria A, Nongkynrih B, Gupta SK (2014) Indoor air pollution in India: implications on health and its control. Indian J Commun Med Off Publ Indian Assoc Prevent Soc Med 39:203–207
4. Medford AJ, Vojvodic A, Hummelshøj JS, Voss J, Abild-Pedersen F, Studt F, Bligaard T, Nilsson A, Nørskov JK (2015) From the Sabatier principle to a predictive theory of transition-metal heterogeneous catalysis. J Catal 328:36–42
5. Rothenberg G (2008) Catalysis: concepts and green applications. Wiley-VCH, Weinheim
6. He C, Cheng J, Zhang X, Douthwaite M, Pattisson S, Hao Z (2019) Recent advances in the catalytic oxidation of volatile organic compounds: a review based on pollutant sorts and sources. Chem Rev 119:4471–4568
7. Zhang Z, Jiang Z, Shangguan W (2016) Low-temperature catalysis for VOCs removal in technology and application: a state-of-the-art review. Catal Today 264:270–278
8. Weon S, He F, Choi W (2019) Status and challenges in photocatalytic nanotechnology for cleaning air polluted with volatile organic compounds: visible light utilization and catalyst deactivation. Environ Sci Nano 6:3185–3214
9. Ollado L, Jansson I, Platero-Prats AE, Perez-Dieste V, Escudero C, Molins E, Doucastela LC et al (2017) Elucidating the photoredox nature of isolated iron active sites on MCM-41. ACS Catal 7:1646–1654
10. Ghoussoub M, Xia M, Duchesne PA, Segal D, Ozin G (2019) Principles of photothermal gas-phase heterogeneous CO_2 catalysis. Energy Environ Sci 12:1122–1142
11. Nair V, Muñoz-Batista MJ, Fernández-García M, Luque R, Colmenares JC (2019) Thermo-photocatalysis: environmental and energy applications. Chemsuschem 12:2098–2116
12. Chen C, Li Y, Yang Y, Zhang Q, Wu J, Xie X, Shi Z, Zhao X (2019) Unique mesoporous amorphous manganese iron oxide with excellent catalytic performance for benzene abatement under UV-vis-IR and IR irradiation. Environ Sci Nano 6:1233–1245

13. Li Y, Han S, Zhang L, Yu Y (2021) Manganese-based catalysts for indoor volatile organic compounds degradation with low energy consumption and high efficiency. In: Transactions of Tianjin University, pp 1–14
14. Meyyappan M (2009) A review of plasma enhanced chemical vapour deposition of carbon nanotubes. J Phys D Appl Phys 42:1–15
15. Gohier A, Minea TM, Djouadi AM, Granier A, Dubosc M (2006) Limits of the PECVD process for single wall carbon nanotubes growth. Chem Phys Lett 421:242–245
16. Gohier A, Minea TM, Djouadi AM, Granier A (2007) Impact of the etching gas on vertically oriented single wall and few walled carbon nanotubes by plasma enhanced chemical vapor deposition. J Appl Phys 101:1–8
17. Neyts EC, Ostrikov K, Sunkara MK, Bogaerts A (2015) Plasma catalysis: synergistic effects at the nanoscale. Chem Rev 115:13408–13446
18. Varanda LC, Morales MP, Jafelicci M, Serna CJ (2002) Monodispersed spindle-type goethite nanoparticles from Fe(III) solutions. J Mater Chem 12:3649–3653
19. Ge S, Shi X, Sun K, Li C, Uher C, Baker JR, Banaszak Holl MM, Orr BG (2009) Facile hydrothermal synthesis of iron oxide nanoparticles with tunable magnetic properties. J Phys Chem C 113:13593–13599
20. KhanFaisal I, Ghoshal AK (2000) Removal of volatile organic compounds from polluted air. J Loss Prevent Process Ind 13:527–545
21. Belessi VC, Ladavos AK, Armatas GS, Pomonis PJ (2001) Kinetics of methane oxidation over La–Sr–Ce–Fe–O mixed oxide solids. Phys Chem Chem Phys 3:3856–3862
22. Ma X, Suo X, Cao H, Guo J, Lv L, Sun H, Zheng M (2014) Deep oxidation of 1, 2-dichlorobenzene over Ti-doped iron oxide. Phys Chem Chem Phys 16:12731–12740
23. Wang G, Wang Y, Qin L, Zhao B, Guo L, Han J (2020) Efficient and stable degradation of chlorobenzene over a porous iron–manganese oxide supported ruthenium catalyst. Catal Sci Technol 10:7203–7216
24. Silva H, Hernandez-Fernandez P, Baden AK, Hellstern HL, Kovyakh A, Wisaeus E, Smitshuysen T et al (2019) Supercritical flow synthesis of PtPdFe alloyed nanoparticles with enhanced low-temperature activity and thermal stability for propene oxidation under lean exhaust gas conditions. Catal Sci Technol 9:6691–6699
25. Fan J, Niu X, Teng W, Zhang P, Zhang W, Zhao D (2020) Highly dispersed Fe–Ce mixed oxide catalysts confined in mesochannels toward low-temperature oxidation of formaldehyde. J Mater Chem A 8:17174–17184
26. Mathew T, Suzuki K, Ikuta Y, Takahashi N, Shinjoh H (2012) Mesoporous ferrihydrite with incorporated manganese for rapid removal of organic contaminants in air. Chem Commun 48:10987–10989
27. Sazama P, Moravkova J, Sklenak S, Vondrova A, Tabor E, Sadovska G, Pilar R (2020) Effect of the nuclearity and coordination of Cu and Fe sites in β zeolites on the oxidation of hydrocarbons. ACS Catal 10:3984–4002
28. Li D, Li K, Xu R, Zhu X, Wei Y, Tian D, Cheng X, Wang H (2019) Enhanced CH_4 and CO Oxidation over $Ce_{1-x}Fe_xO_{2-\delta}$ hybrid catalysts by tuning the lattice distortion and the state of surface iron species. ACS Appl Mater Interf 11:19227–19241
29. House MP, Carley AF, Echeverria-Valda R, Bowker M (2008) Effect of varying the cation ratio within iron molybdate catalysts for the selective oxidation of methanol. J Phys Chem C 112:4333–4341
30. Mao J, He D, Zhao Y, Zhang L, Luo Y (2022) Sulfur-resistance iron catalyst in sulfur-containing VOCs abatement modulated through H_2 reduction. Appl Surf Sci 584(152631):1–11
31. Xue T, Li R, Gao Y, Wang Q (2020) Iron mesh-supported vertically aligned Co–Fe layered double oxide as a novel monolithic catalyst for catalytic oxidation of toluene. Chem Eng J 384:1–35
32. Bonelli R, Albonetti S, Morandi V, Ortolani L, Riccobene PM, Scirè S, Zacchini S (2011) Design of nano-sized FeO_x and Au/FeO_x catalysts supported on CeO_2 for total oxidation of VOC. Appl Catal A Gen 395:10–18

33. Guo M, Li K, Zhang H, Min X, Liang J, Hu X, Guo W, Jia J, Sun T (2020) Promotional removal of oxygenated VOC over manganese-based multi oxides from spent lithium-ions manganate batteries: modification with Fe, Bi and Ce dopants. Sci Total Environ 740:1–43
34. Xia H, Chen Y, Wu J, Shao S, Chen G, Zhang H, Dai Q, Wang X (2021) Oxidative decomposition of chlorobenzene over iron titanate catalysts: the critical roles of oxygen vacancies and adsorption geometries. Appl Catal A Gen 617:1–9
35. Xia Y, Wang Z, Feng Y, Xie S, Liu Y, Dai H, Deng J (2020) In situ molten salt derived iron oxide supported platinum catalyst with high catalytic performance for o-xylene elimination. Catal Today 351:30–36
36. Das DP, Parida KM (2007) Fe(III) oxide pillared titanium phosphate (TiP): an effective catalyst for deep oxidation of VOCs. J Mol Catal A Chem 276:17–23
37. Sanchis R, Dejoz A, Vázquez I, Vilarrasa-García E, Jiménez-Jiménez J, Rodríguez-Castellón E, López Nieto JM, Solsona B (2019) Ferric sludge derived from the process of water purification as an efficient catalyst and/or support for the removal of volatile organic compounds. Chemosphere 219:286–295
38. Xue T, Li R, Zhang Z, Gao Y, Wang Q (2020) Preparation of MnO_2 decorated $Co_3Fe_1O_x$ powder/monolithic catalyst with improved catalytic activity for toluene oxidation. J Environ Sci 96:194–203
39. Tsoncheva T, Ivanova R, Henych J, Velinov N, Kormunda M, Dimitrov M, Paneva D, Slušná M, Mitov I, Štengl V (2016) Iron modified titanium–hafnium binary oxides as catalysts in total oxidation of ethyl acetate. Catal Commun 81:14–19
40. Li D, Li C, Suzuki K (2013) Catalytic oxidation of VOCs over Al-and Fe-pillared montmorillonite. Appl Clay Sci 77:56–60
41. Durán FG, Barbero BP, Cadús LE, Rojas C, Centeno MA, Odriozola JA (2009) Manganese and iron oxides as combustion catalysts of volatile organic compounds. Appl Catal B Environ 92:194–201
42. Nogueira FGE, Lopes JH, Silva AC, Lago RM, Fabris JD, Oliveira LCA (2011) Catalysts based on clay and iron oxide for oxidation of toluene. Appl Clay Sci 51:385–389
43. Yang K, Liu Y, Deng J, Zhao X, Yang J, Han Z, Hou Z, Dai H (2019) Three-dimensionally ordered mesoporous iron oxide-supported single-atom platinum: highly active catalysts for benzene combustion. Appl Catal B Environ 244:650–659
44. Minicò S, Scirè S, Crisafulli C, Maggiore R, Galvagno S (2000) Catalytic combustion of volatile organic compounds on gold/iron oxide catalysts. Appl Catal B Environ 28:245–251
45. Wang HC, Liang HS, Chang MB (2011) Chlorobenzene oxidation using ozone over iron oxide and manganese oxide catalysts. J Hazard Mater 186:1781–1787
46. Tsoncheva T, Ivanova R, Dimitrov M, Paneva D, Kovacheva D, Henych J, Vomáčka P et al (2016) Template-assisted hydrothermally synthesized iron-titanium binary oxides and their application as catalysts for ethyl acetate oxidation. Appl Catal A Gen 528:24–35
47. Wang Y, Wang G, Deng W, Han J, Qin L, Zhao B, Guo L, Xing F (2020) Study on the structure-activity relationship of Fe–Mn oxide catalysts for chlorobenzene catalytic combustion. Chem Eng J 395(125172):1–13
48. Xia Y, Dai H, Jiang H, Zhang L, Deng J, Liu Y (2011) Three-dimensionally ordered and wormhole-like mesoporous iron oxide catalysts highly active for the oxidation of acetone and methanol. J Hazard Mater 186:84–91
49. Morales MR, Barbero BP, Cadús LE (2007) Combustion of volatile organic compounds on manganese iron or nickel mixed oxide catalysts. Appl Catal B Environ 74:1–10
50. Hammiche-Bellal Y, Zouaoui-Mahzoul N, Lounas I, Benadda A, Benrabaa R, Auroux A, Meddour-Boukhobza L, Djadoun A (2017) Cobalt and cobalt–iron spinel oxides as bulk and silica supported catalysts in the ethanol combustion reaction. J Mol Catal A Chem 426:97–106
51. Li Z, Yan Q, Jiang Q, Gao Y, Xue T, Li R, Liu Y, Wang Q (2020) Oxygen vacancy mediated $Cu_yCo_{3-y}Fe_1O_x$ mixed oxide as highly active and stable toluene oxidation catalyst by multiple phase interfaces formation and metal doping effect. Appl Catal B Environ 269:1–13
52. Djinović P, Ristić A, Žumbar T, Dasireddy VDBC, Rangus M, Dražić M, Popova M, Likozar B, Logar MZ, Tušar NN (2020) Synergistic effect of CuO nanocrystals and Cu-oxo-Fe clusters

on silica support in promotion of total catalytic oxidation of toluene as a model volatile organic air pollutant. Appl Catal B Environ 268:1–30
53. Li C, Shen Y, Jia M, Sheng S, Adebajo MO, Zhu H (2008) Catalytic combustion of formaldehyde on gold/iron-oxide catalysts. Catal Commun 9:355–361
54. Sanchis R, Cecilia JA, Soriano MD, Vázquez MI, Dejoz A, Nieto JML, Rodríguez Castellón E, Solsona B (2018) Porous clays heterostructures as supports of iron oxide for environmental catalysis. Chem Eng J 334:1159–1168
55. Ma X, Wen J, Guo H, Ren G (2020) Facile template fabrication of Fe–Mn mixed oxides with hollow microsphere structure for efficient and stable catalytic oxidation of 1,2-dichlorobenzene. Chem Eng J 382:1–41
56. Chen J, Chen X, Xu W, Xu Z, Chen J, Jia H, Chen J (2017) Hydrolysis driving redox reaction to synthesize Mn–Fe binary oxides as highly active catalysts for the removal of toluene. Chem Eng J 330:281–293
57. Liang X, Qi F, Liu P, Wei G, Su X, Ma L, He H et al (2016) Performance of Ti-pillared montmorillonite supported Fe catalysts for toluene oxidation: the effect of Fe on catalytic activity. Appl Clay Sci 132:96–104
58. Collado L, Jansson I, Platero-Prats AE, Perez-Dieste V (2017) Carlos eof isolated iron active sites on MCM-41. ACS Catal 7:1646–1654
59. Saqlain S, Cha BJ, Kim SY, Ahn TK, Park C, Oh JM, Jeong EC, Seo HO, Kim YD (2020) Visible light-responsive Fe-loaded TiO_2 photocatalysts for total oxidation of acetaldehyde: fundamental studies towards large-scale production and applications. Appl Surf Sci 505:1–9
60. Soltani T, Lee BK (2017) Comparison of benzene and toluene photodegradation under visible light irradiation by Ba-doped $BiFeO_3$ magnetic nanoparticles with fast sonochemical synthesis. Photochem Photobiol Sci 16:86–95
61. Chen X, Zhu H-Y, Zhao J-C, Zheng Z-F, Gao X-P (2008) Visible-light-driven oxidation of organic contaminants in air with gold nanoparticle catalysts on oxide supports. Angew Chem 120:5433–5436
62. Wu H, Wang L (2014) Phase transformation-induced crystal plane effect of iron oxide micropine dendrites on gaseous toluene photocatalytic oxidation. Appl Surf Sci 288:398–404
63. Tabari T, Singh D, Jamali SS (2017) Enhanced photocatalytic activity of mesoporous $ZnFe_2O_4$ nanoparticles towards gaseous benzene under visible light irradiation. J Environ Chem Eng 5:931–939
64. Kim SY, Saqlain S, Cha BJ, Zhao S, Seo HO, Kim YD (2020) Annealing temperature-dependent effects of Fe-loading on the visible light-driven photocatalytic activity of rutile TiO_2 nanoparticles and their applicability for air purification. Catalysts 10:1–18
65. Low W, Boonamnuayvitaya V (2013) Enhancing the photocatalytic activity of TiO_2 co-doping of graphene—Fe^{3+} ions for formaldehyde removal. J Environ Manag 127:142–149
66. Wang H, Raziq F, Qu Y, Qin C, Wang J, Jing L (2015) Role of quaternary *N* in *N*-doped graphene—Fe_2O_3 nanocomposites as efficient photocatalysts for CO_2 reduction and acetaldehyde degradation. RSC Adv 5:85061–85064
67. Liu J, Liu X, Chen J, Li X, Zhong F (2021) Plasma-catalytic oxidation of toluene on Fe_2O_3/sepiolite catalyst in DDBD reactor. J Phys D Appl Phys 54(475201):1–13
68. Trinh QH, Mok YS (2015) Non-thermal plasma combined with cordierite-supported Mn and Fe based catalysts for the decomposition of diethylether. Catalysts 5:800–814
69. Sultana S, Ye Z, Veerapandian SKP, Löfberg A, De Geyter N, Morent R, Giraudon JM, Lamonier JF (2018) Synthesis and catalytic performances of K-OMS-2, Fe/K-OMS-2 and Fe-K-OMS-2 in post plasma-catalysis for dilute TCE abatement. Catal Today 307:20–28
70. Cai Y, Zhu X, Hu W, Zheng C, Yang Y, Chen M, Gao X (2019) Plasma-catalytic decomposition of ethyl acetate over $LaMO_3$ (M= Mn, Fe, and Co) perovskite catalysts. J Ind Eng Chem 70:447–452
71. Qin L, Zhao B, Chen W, Liu X, Han J (2022) Refluxing-coprecipitation to synthesize Fe_x–Mn_y/γ-Al_2O_3 catalyst for toluene removal in a nonthermal plasma-catalysis reactor. Mol Catal 517:1–14

72. Liu J, Liu X, Chen J, Li X, Ma T, Zhong F (2021) Investigation of ZrMnFe/sepiolite catalysts on toluene degradation in a one-stage plasma-catalysis system. Catalysts 11(828):1–12
73. Al Soubaihi RM, Saoud KM, Dutta J (2018) Critical review of low-temperature CO oxidation and hysteresis phenomenon on heterogeneous catalysts. Catalysts 8:1–19
74. Haruta M (2004) Gold as a novel catalyst in the 21st century: preparation, working mechanism and applications. Gold Bull 37:27–36
75. Pan C-J, Tsai MC, Su WN, Rick J, Akalework NG, Agegnehu AK, Cheng SY, Hwang BJ (2017) Tuning/exploiting strong metal-support interaction (SMSI) in heterogeneous catalysis. J Taiwan Instit Chem Eng 74:154–186
76. Sun YN, Qin ZH, Lewandowski M, Carrasco E, Sterrer M, Shaikhutdinov S, Freund HJ (2009) Monolayer iron oxide film on platinum promotes low temperature CO oxidation. J Catal 266:359–368
77. Carrettin S, Hao Y, Aguilar-Guerrero V, Gates BC, Trasobares S, Calvino JJ, Corma A (2007) Increasing the number of oxygen vacancies on TiO_2 by doping with iron increases the activity of supported gold for CO oxidation. Chem A Eur J 13:7771–7779
78. Biabani-Ravandi A, Rezaei M, Fattah Z (2013) Low-temperature CO oxidation over nanosized Fe–Co mixed oxide catalysts: effect of calcination temperature and operational conditions. Chem Eng Sci 94:237–244
79. Ciambelli P, Stefano Cimino S, De Rossi LL, Minelli G, Porta P, Russo G (2001) $AFeO_3$ (A= La, Nd, Sm) and $LaFe_{1-x}Mg_xO_3$ perovskites as methane combustion and CO oxidation catalysts: structural, redox and catalytic properties. Appl Catal B Environ 29:239–250
80. Yamamoto TA, Nakagawa T, Seino S, Nitani H (2010) Bimetallic nanoparticles of PtM (M= Au, Cu, Ni) supported on iron oxide: radiolytic synthesis and CO oxidation catalysis. Appl Catal A Gen 387:195–202
81. Zheng B, Gan T, Shi S, Wang J, Zhang W, Zhou X, Zou Y, Yan W, Liu G (2021) Exsolution of iron oxide on $LaFeO_3$ Perovskite: a robust heterostructured support for constructing self-adjustable Pt-based room-temperature CO oxidation catalysts. ACS Appl Mater Interf 13:27029–27040
82. Moreau F, Bond GC (2006) CO oxidation activity of gold catalysts supported on various oxides and their improvement by inclusion of an iron component. Catal Today 114:362–368
83. Cheng T, Fang Z, Hu Q, Han K, Yang X, Zhang Y (2007) Low-temperature CO oxidation over CuO/Fe_2O_3 catalysts. Catal Commun 8:1167–1171
84. Cao J, Wang Y, Ma T, Liu Y, Yuan Z (2011) Synthesis of porous hematite nanorods loaded with CuO nanocrystals as catalysts for CO oxidation. J Nat Gas Chem 20:669–676
85. Biabani-Ravandi A, Rezaei M, Fattah Z (2013) Study of Fe–Co mixed metal oxide nanoparticles in the catalytic low-temperature CO oxidation. Process Saf Environ Protect 91:489–494
86. Liu G, Walsh AG, Zhang P (2020) Synergism of iron and platinum species for low-temperature CO oxidation: from two-dimensional surface to nanoparticle and single-atom catalysts. J Phys Chem Lett 11:2219–2229
87. Kast P, Friedrich M, Teschner D, Girgsdies F, Lunkenbein T, D'Alnoncourt RN, Behrens M, Schlögl R (2015) CO oxidation as a test reaction for strong metal–support interaction in nanostructured Pd/FeO_x powder catalysts. Appl Catal A Gen 502:8–17
88. Li P, Miser DE, Rabiei S, Yadav RT, Hajaligol MR (2003) The removal of carbon monoxide by iron oxide nanoparticles. Appl Catal B Environ 43:151–162
89. Wu Y, Dong L, Li B (2018) Effect of iron on physicochemical properties: enhanced catalytic performance for novel Fe_2O_3 modified $CuO/Ti_{0.5}Sn_{0.5}O_2$ in low temperature CO oxidation. Mol Catal 456:65–74
90. Carriazo JG, Martinez LM, Odriozola JA, Moreno S, Molina R, Centeno MA (2007) Gold supported on Fe, Ce, and Al pillared bentonites for CO oxidation reaction. Appl Catal B Environ 72:157–165
91. Carabineiro SAC, Bogdanchikova N, Tavares PB, Figueiredo JL (2012) Nanostructured iron oxide catalysts with gold for the oxidation of carbon monoxide. RSC Adv 2:2957–2965

92. Hinojosa-Reyes M, Camposeco-Solis R, Zanella R, Rodríguez-González V, Ruiz F (2018) Gold nanoparticle: enhanced CO oxidation at low temperatures by using Fe-doped TiO_2 as support. Catal Lett 148:383–396
93. Falls A, Seinfeld J (1978) Continued development of a kinetic mechanism for photochemical smog. Environ Sci Technol 12:1398–1406
94. Wang J, Tian GL, Cui SP, Wang YL (2018) Different precipitant preparation of nickel-doped Mn/TiO_2 catalysts for low-temperature SCR of NO with NH_3. Mater Sci Forum 913:976–984
95. Dumesic JA, Topsøe N-Y, Topsøe H, Chen Y, Slabiak T (1996) Kinetics of selective catalytic reduction of nitric oxide by ammonia over vanadia/titania. J Catal 163:409–417
96. Busca G, Lietti L, Ramis G, Berti F (1998) Chemical and mechanistic aspects of the selective catalytic reduction of NO_x by ammonia over oxide catalysts: a review. Appl Catal B Environ 18:1–36
97. Tounsi H, Djemal S, Petitto C, Delahay G (2011) Copper loaded hydroxyapatite catalyst for selective catalytic reduction of nitric oxide with ammonia. Appl Catal B Environ 107:158–163
98. Dunn JP, Koppula PR, Stenger HG, Wachs IE (1998) Oxidation of sulfur dioxide to sulfur trioxide over supported vanadia catalysts. Appl Catal B Environ 19:103–117
99. Cai S, Zhang D, Zhang L, Huang L, Li H, Gao R, Shi L, Zhang J (2014) Comparative study of 3D ordered macroporous $Ce_{0.75}Zr_{0.2}M_{0.05}O_2$ (M = Fe, Cu, Mn, Co) for selective catalytic reduction of NO with NH_3. Catal Sci Technol 4:93–101
100. Chen Z, Wang F, Li H, Yang Q, Wang L, Li X (2012) Low-temperature selective catalytic reduction of NOx with NH_3 over Fe–Mn mixed-oxide catalysts containing $Fe_3Mn_3O_8$ phase. Ind Eng Chem Res 51:202–212
101. Liu F, He H, Zhang C, Feng Z, Zheng L, Xie Y, Hu T (2010) Selective catalytic reduction of NO with NH_3 over iron titanate catalyst: catalytic performance and characterization. Appl Catal B 96:408–420
102. Yu J, Guo F, Wang Y, Zhu J, Liu Y, Su F, Gao S, Xu G (2010) Sulfur poisoning resistant mesoporous Mn-base catalyst for low-temperature SCR of NO with NH_3. Appl Catal B 95:160–168
103. Cai S, Zhang D, Shi L, Xu J, Zhang L, Huang L, Li H, Zhang J (2014) Porous Ni–Mn oxide nanosheets in situ formed on nickel foam as 3D hierarchical monolith de-NO_x catalysts. Nanoscale 6:7346–7353
104. Zhang S, Zhang B, Liu B, Sun S (2017) A review of Mn-containing oxide catalysts for low temperature selective catalytic reduction of NO_x with NH_3: reaction mechanism and catalyst deactivation. RSC Adv 7:26226–26242
105. Li X, Li J, Peng Y, Zhang T, Liu S, Hao J (2015) Selective catalytic reduction of NO with NH_3 over novel iron–tungsten mixed oxide catalyst in a broad temperature range. Catal Sci Technol 5:4556–4564
106. Li Y, Wan Y, Li Y, Zhan S, Guan Q, Tian Y (2016) Low-temperature selective catalytic reduction of NO with NH_3 over Mn_2O_3-doped Fe_2O_3 hexagonal microsheets. ACS Appl Mater Interf 8:5224–5233
107. Yang S, Qi F, Xiong S, Dang H, Liao Y, Wong PK, Li J (2016) MnO_x supported on Fe–Ti spinel: a novel Mn based low temperature SCR catalyst with a high N_2 selectivity. Appl Catal B Environ 181:570–580
108. Ko S, Tang X, Gao F, Wang C, Liu H, Liu Y (2022) Selective catalytic reduction of NO_x with NH_3 on Mn, Co-BTC-derived catalysts: influence of thermal treatment temperature. J Solid State Chem 307:1–9
109. Zhan S, Qiu M, Yang S, Zhu D, Yu H, Li Y (2014) Facile preparation of MnO_2 doped Fe_2O_3 hollow nanofibers for low temperature SCR of NO with NH_3. J Mater Chem A 2:20486–20493
110. Li Y, Li Y, Wang P, Hu W, Zhang S, Shi Q, Zhan S (2017) Low-temperature selective catalytic reduction of NO_x with NH_3 over $MnFeO_x$ nanorods. Chem Eng J 330:213–222
111. Gao C, Xiao B, Shi JW, He C, Wang B, Ma D, Cheng Y, Niu C (2019) Comprehensive understanding the promoting effect of Dy-doping on $MnFeO_x$ nanowires for the low-temperature NH_3-SCR of NO_x: an experimental and theoretical study. J Catal 380:55–67

112. Shao C, Liu X, Meng D, Xu Q, Guo Y, Guo Y, Zhan W, Wang L, Lu G (2016) Catalytic performance of Co–Fe mixed oxide for NH_3-SCR reaction and the promotional role of cobalt. RSC Adv 6:66169–66179
113. Sun J, Lu Y, Zhang L, Ge C, Tang C, Wan H, Dong L (2017) Comparative study of different doped metal cations on the reduction, acidity, and activity of $Fe_9M_1O_x$ (M= Ti^{4+}, $Ce^{4+/3+}$, Al^{3+}) catalysts for NH_3-SCR reaction. Ind Eng Chem Res 56:12101–12110
114. Wang H, Ning P, Zhang Y, Ma Y, Wang J, Wang L, Zhang Q (2020) Highly efficient WO_3-FeO_x catalysts synthesized using a novel solvent-free method for NH_3-SCR. J Hazard Mater 388(121812):1–35
115. Wei Y, Chen Y, Wang R (2018) Rare earth salt of 12-tungstophosphoric acid supported on iron oxide as a catalyst for selective catalytic reduction of NO_x. Fuel Process Technol 178:262–270
116. Yao H, Cai S, Yang B, Han L, Wang P, Li H, Yan T, Shi L, Zhang D (2020) In situ decorated MOF-derived Mn–Fe oxides on Fe mesh as novel monolithic catalysts for NO_x reduction. New J Chem 44:2357–2366
117. Jia J, Ran R, Guo X, Wu X, Chen W, Weng D (2019) Enhanced low-temperature NO oxidation by iron-modified MnO_2 catalysts. Catal Commun 119:139–143
118. Zhang Y, Xu Z, Wang X, Lu X, Zheng Y (2015) Fabrication of Mn-FeO_x/CNTs catalysts for low-temperature NO reduction with NH_3. NANO 10:1–9
119. Wei L, Li X, Mu J, Wang X, Fan S, Yin Z, Tadé MO, Liu S (2020) Rationally tailored redox properties of a mesoporous Mn–Fe spinel nanostructure for boosting low-temperature selective catalytic reduction of NO_x with NH_3. ACS Sustainable Chem Eng 8:17727–17739
120. Ochando-Pulido JM, Pimentel-Moral S, Verardo V, Martinez-Ferez A (2017) A focus on advanced physicochemical processes for olive mill wastewater treatment. Separ Purif Technol 179:161–174
121. Karthikeyan S, Titus A, Gnanamani A, Mandal AB, Sekaran G (2011) Treatment of textile wastewater by homogeneous and heterogeneous Fenton oxidation processes. Desalination 281:438–445
122. Kishimoto N, Kitamura T, Kato M, Otsu H (2013) Reusability of iron sludge as an iron source for the electrochemical Fenton-type process using Fe^{2+}/HOCl system. Water Res 47:1919–1927
123. Babuponnusami A, Muthukumar K (2014) A review of Fenton and improvements to the Fenton process for wastewater treatment. J Environ Chem Eng 2:557–572
124. Garcia-Segura S, Bellotindos LM, Huang Y-H, Brillas E, Lu M-C (2016) Fluidized-bed Fenton process as alternative wastewater treatment technology: a review. J Taiwan Inst Chem Eng 67:211–225
125. Queiros S, Morais V, Rodrigues CSD, Maldonado-Hodar FJ, Madeira LM (2015) Heterogeneous Fenton's oxidation using Fe/ZSM-5 as catalyst in a continuous stirred tank reactor. Separ Purif Technol 141:235–245
126. Vorontsov AV (2019) Advancing Fenton and photo-Fenton water treatment through the catalyst design. J Hazard Mater 372:103–112
127. Poza-Nogueiras V, Rosales E, Pazos M, Sanroman MA (2018) Current advances and trends in electro-Fenton process using heterogeneous catalysts: a review. Chemosphere 201:399–416
128. Dulova N, Trapido M, Dulov A (2011) Catalytic degradation of picric acid by heterogeneous Fenton: based processes. Environ Technol 32:439–446
129. Casado J (2019) Towards industrial implementation of electro-Fenton and derived technologies for wastewater treatment: a review. J Environ Chem Eng 7:1–62
130. He Z, Gao C, Qian M, Shi Y, Chen J, Song S (2014) Electro-Fenton process catalyzed by Fe_3O_4 magnetic nanoparticles for degradation of C.I. reactive blue 19 in aqueous solution: operating conditions, influence, and mechanism. Ind Eng Chem Res 53:3435–3447
131. Ben Hafaiedh N, Fourcade F, Bellakhal N, Amrane A (2020) Iron oxide nanoparticles as heterogeneous electro-Fenton catalysts for the removal of AR18 azo dye. Environ Technol 41:2146–2153
132. Baiju A, Gandhimathi R, Ramesh ST, Nidheesh PV (2018) Combined heterogeneous electro-Fenton and biological process for the treatment of stabilized landfill leachate. J Environ Manag 210:328–337

133. Huang B, Qi C, Yang Z, Guo Q, Chen W, Zeng G, Lei C (2017) Pd/Fe_3O_4 nanocatalysts for highly effective and simultaneous removal of humic acids and Cr(VI) by electro-Fenton with H_2O_2 in situ electro-generated on the catalyst surface. J Catal 352:337–350
134. Barhoumi N, Olvera-Vargas H, Oturan N, Huguenot D, Gadri A, Ammar S, Brillas E, Oturan MA (2017) Kinetics of oxidative degradation/mineralization pathways of the antibiotic tetracycline by the novel heterogeneous electro-Fenton process with solid catalyst chalcopyrite. Appl Catal B Environ 209:637–647
135. Barhoumi N, Labiadh L, Oturan MA, Oturan N, Gadri A, Ammar S, Brillas E (2015) Electrochemical mineralization of the antibiotic levofloxacin by electro-Fenton-pyrite process. Chemosphere **141**:250–257